

Anomalous Higgs couplings in $e\gamma$ collision with initial beam and final state polarizations

İnanç Şahin*

*Department of Physics, Faculty of Sciences,
Ankara University, 06100 Tandoğan, Ankara, Turkey*

Abstract

We investigate the constraints on the anomalous WWH couplings through the process $e^-\gamma \rightarrow \nu_e W^- H$. Considering incoming beam polarizations and the longitudinal and transverse polarization states of the final W boson, we find 95% confidence level limits on the anomalous coupling parameters with an integrated luminosity of 500 fb^{-1} and $\sqrt{s} = 0.5$ and 1 TeV energy. We show that initial beam and final state polarizations highly improve the sensitivity limits of the anomalous coupling parameters b_W and β_W .

PACS numbers: 12.15.Ji, 12.60.Fr, 13.88.+e

*isahin@science.ankara.edu.tr

I. INTRODUCTION

The Standard model (SM) of particle physics has been proven to be successful in the energy scale of the present colliders. Experimental results obtained from recent experiments at CERN LEP and Fermilab Tevatron confirm the $SU(3)_C \times SU(2)_L \times U(1)_Y$ gauge structure of SM. However, the Higgs boson which is crucial for electroweak symmetry breaking and mass generation has not been observed, and one of the main goals of future experiments is to pursue its trace. Although the exact value of the Higgs mass is unknown there are experimental bounds for it. Direct searches from ALEPH, DELPHI, L3, and OPAL collaborations at CERN LEP provide a lower bound on the Higgs mass of $m_H > 114.4$ GeV [1]. Indirect experimental bounds for the Higgs mass are obtained from fits to precision measurements of electroweak observables. The current best fit value sets an upper bound of $m_H < 186$ GeV [2].

If a Higgs boson is detected at future TeV scale colliders, it will be crucial to test its couplings to the SM particles. Precision measurements of Higgs couplings may give us some hints for new physics beyond the SM. It is argued that CERN LHC has a potential to search for the Higgs boson in the entire mass range allowed. In case it is found at CERN LHC, precision measurements of its couplings to the SM particles can be obtained at future linear e^+e^- colliders. After linear e^+e^- colliders are constructed its operating modes of $e\gamma$ and $\gamma\gamma$ are expected to be designed [3]. A real gamma beam is obtained through Compton backscattering of laser light off the linear electron beam where most of the photons are produced at the high energy region. The luminosities for $e\gamma$ and $\gamma\gamma$ collisions turn out to be of the same order as the one for e^+e^- [4], so the cross sections for photoproduction processes with real photons are considerably larger than the virtual photon case. Polarizability of the real gamma beam is an additional advantage for polarized beam experiments. Therefore $e\gamma$ and $\gamma\gamma$ collisions should be discussed as complementary to e^+e^- collisions.

In this work we analyzed the anomalous WWH vertex in the $e\gamma$ collision. We consider the process $e^-\gamma \rightarrow \nu_e W^- H$. This process isolates the WWH vertex and gives us the opportunity to study the WWH vertex independent from ZZH . On the other hand in e^+e^- collisions, observables depending on WWH also receive contributions from the ZZH and it is very difficult to dissociate WWH from ZZH [5].

Anomalous WWH couplings can be investigated in a model independent way by means

of the effective Lagrangian approach [5, 6, 7, 8]. In writing effective operators we employ the formalism of [5, 8]. Imposing Lorentz invariance and gauge invariance and retaining up to dimension six operators in the effective Lagrangian, the most general coupling structure is expressed as,

$$\Gamma_{\mu\nu}^V = i\tilde{g}_V \left[a_V g_{\mu\nu} + \frac{b_V}{m_V^2} (k_{2\mu} k_{1\nu} - g_{\mu\nu} k_1 \cdot k_2) + \frac{\beta_V}{m_V^2} \epsilon_{\mu\nu\alpha\beta} k_1^\alpha k_2^\beta \right] \quad (1)$$

with

$$\tilde{g}_W = g_W m_W, \quad \tilde{g}_Z = \frac{g_W m_W}{\cos^2 \theta_W}, \quad g_W = \frac{g_e}{\sin \theta_W}, \quad g_e = \sqrt{4\pi\alpha} \quad (2)$$

where k_1^μ and k_2^μ represent the momentum of two W or Z boson (V=W, Z). For a convention we assume that all the momenta are outgoing from the vertex. Within the standard model at tree level, the couplings are given by $a_V = 1$, $b_V = 0$, and $\beta_V = 0$.

In the literature there have been several studies for anomalous WWH couplings. The LHC will start operating soon. Anomalous gauge couplings of the Higgs boson have been studied at the LHC via the weak-boson scattering [9] and vector boson fusion [10] processes. There has been a great amount of work on anomalous WWH couplings which focus on the future linear e^+e^- collider and its $e\gamma$ and $\gamma\gamma$ modes. Anomalous WWH couplings have been analyzed through the processes $e^+e^- \rightarrow f\bar{f}H$ [5, 7], $e^+e^- \rightarrow W^+W^-\gamma$ [11], $e^-\gamma \rightarrow \nu_e W^-H$ [8], and $\gamma\gamma \rightarrow WWW$ [12].

The anomalous cross sections are quadratic functions of the anomalous parameters α_j ($j = 1, 2, \dots$) i.e.,

$$\sigma_{AN} = \sigma_{SM} + \alpha_j \sigma_{int}^j + \alpha_j^2 \sigma_{ano}^j + \alpha_j \alpha_i \sigma_{ano}^{ji}$$

where σ_{SM} is the SM cross section, σ_{int}^j is the interference term between the SM and the anomalous contribution, and σ_{ano}^j and σ_{ano}^{ji} are the pure anomalous contributions. In Ref. [8] authors ignore quadratic anomalous coupling terms in the cross section calculations; they retain contributions only up to the lowest nontrivial order, i.e. $\alpha_j \sigma_{int}^j$. This is reasonable due to the higher dimensional nature of their origin. On the other hand, these quadratic terms generally have a higher momentum dependence than linear terms and may have a significant contribution at high energies. For example, in the anomalous WWH vertex (1) coefficients

of $\frac{b_W}{m_W^2}$ and $\frac{\beta_W}{m_W^2}$ have a momentum dependence of dimension 2. Therefore in the anomalous cross section for the process $e^-\gamma \rightarrow \nu_e W^- H$, the contributions σ_{ano}^j contain two additional momentum dependence when we compare with σ_{int}^j . Of course the terms σ_{ano}^j are suppressed by the inverse powers of new physics energy scale (NPS) but their contribution grows faster than the contribution of σ_{int}^j as the energy increases and approaches NPS. Therefore these quadratic anomalous contributions should be considered at high energy processes. We will consider all anomalous terms in our tree-level cross section calculations.

As in Ref. [8], we take into account initial electron and photon polarizations before Compton backscattering. Furthermore we take into account initial electron beam polarization which takes part in the subprocess and also the final state polarizations of W boson. We will show that these polarization configurations which have not been considered in Ref. [8] lead to a significant amount of improvement in the sensitivity limits.

II. POLARIZED CROSS SECTIONS

The process $e^-\gamma \rightarrow \nu_e W^- H$ takes part as a subprocess in the e^+e^- collision. A real gamma beam which enters the subprocess is obtained through Compton backscattering of laser light off linear electron or positron beam.

The spectrum of backscattered photons in connection with helicities of initial laser photon and electron is given by [4]

$$f_{\gamma/e}(y) = \frac{1}{g(\zeta)} \left[1 - y + \frac{1}{1-y} - \frac{4y}{\zeta(1-y)} + \frac{4y^2}{\zeta^2(1-y)^2} + \lambda_0 \lambda_e r \zeta (1-2r)(2-y) \right] \quad (3)$$

where

$$g(\zeta) = g_1(\zeta) + \lambda_0 \lambda_e g_2(\zeta) \quad (4)$$

$$g_1(\zeta) = \left(1 - \frac{4}{\zeta} - \frac{8}{\zeta^2} \right) \ln(\zeta+1) + \frac{1}{2} + \frac{8}{\zeta} - \frac{1}{2(\zeta+1)^2}$$

$$g_2(\zeta) = \left(1 + \frac{2}{\zeta} \right) \ln(\zeta+1) - \frac{5}{2} + \frac{1}{\zeta+1} - \frac{1}{2(\zeta+1)^2} \quad (5)$$

Here $r = y/[\zeta(1-y)]$ and $\zeta = 4E_e E_0/M_e^2$. E_0 and λ_0 are the energy and the helicity of the initial laser photon and E_e and λ_e are the energy and the helicity of the initial electron beam before Compton backscattering. y is the fraction which represents the ratio between

the scattered photon and initial electron energy for the backscattered photons moving along the initial electron direction. The maximum value of y reaches 0.83 when $\zeta = 4.8$ in which the backscattered photon energy is maximized without spoiling the luminosity.

Backscattered photons are not in fixed helicity states. Their helicities are described by a distribution :

$$\xi(E_\gamma, \lambda_0) = \frac{\lambda_0(1-2r)(1-y+1/(1-y)) + \lambda_e r \zeta [1 + (1-y)(1-2r)^2]}{1-y+1/(1-y) - 4r(1-r) - \lambda_e \lambda_0 r \zeta (2r-1)(2-y)} \quad (6)$$

The helicity dependent differential cross section for the subprocess can be connected to initial laser photon helicity λ_0 and initial electron beam polarization P_e through the formula

$$\begin{aligned} d\hat{\sigma}(\lambda_0, P_e; \lambda_W) &= \frac{1}{4}(1-P_e) [(1+\xi(E_\gamma, \lambda_0))d\hat{\sigma}(+, L; \lambda_W) + (1-\xi(E_\gamma, \lambda_0))d\hat{\sigma}(-, L; \lambda_W)] \\ &+ \frac{1}{4}(1+P_e) [(1+\xi(E_\gamma, \lambda_0))d\hat{\sigma}(+, R; \lambda_W) + (1-\xi(E_\gamma, \lambda_0))d\hat{\sigma}(-, R; \lambda_W)] \end{aligned} \quad (7)$$

Here $d\hat{\sigma}(\lambda_\gamma, \sigma; \lambda_W)$ is the helicity dependent differential cross section in the helicity eigenstates; $\sigma : L, R$, $\lambda_\gamma = +, -$ and $\lambda_W = +, -, 0$. It should be noted that P_e and λ_e refer to different beams. P_e is the electron beam polarization which enters the subprocess but λ_e is the polarization of initial electron beam before Compton backscattering.

The integrated cross section over the backscattered photon spectrum is

$$d\sigma(\lambda_0, P_e; \lambda_W) = \int_{y_{min}}^{0.83} f_{\gamma/e}(y) d\hat{\sigma}(\lambda_0, P_e; \lambda_W) dy \quad (8)$$

where $y_{min} = \frac{(m_W+m_H)^2}{s}$.

The process $e^- \gamma \rightarrow \nu_e W^- H$ is described by three tree-level diagrams (Fig.1). Each of the diagrams contains an anomalous WWH vertex. The helicity amplitudes have been calculated using vertex amplitude techniques derived in Ref. [13] and the phase space integrations have been performed by GRACE [14] which uses a Monte Carlo routine.

In our calculations we choose to work with a Higgs boson of mass 120 GeV which is compatible with current mass bounds. We accept that initial electron beam polarizability is $|\lambda_e|, |P_e|=0.8$. To see the influence of initial beam polarization, energy distribution of

backscattered photons $f_{\gamma/e}$ is plotted for $\lambda_e \lambda_0 = 0, -0.8$, and $+0.8$ in Fig.2. We see from the figure that backscattered photon distribution is very low at high energies in $\lambda_e \lambda_0 = +0.8$. Therefore we will only consider the case $\lambda_e \lambda_0 < 0$ in the cross section calculations.

One can see from Figs.3-5 the influence of the initial state polarizations on the deviations of the total cross sections from their SM value. In Fig.3 initial polarization configurations $(\lambda_e, \lambda_0, P_e) = (+0.8, -1, \mp 0.8)$ are omitted since they coincide with $(\lambda_e, \lambda_0, P_e) = (-0.8, +1, \mp 0.8)$. We see from Figs. 3-5 that cross section is very sensitive to P_e . This is reasonable due to $V-A$ structure of the $W e \nu_e$ vertex in the Feynman diagrams. Deviation of the cross section from its SM value reaches its maximum at the $(\lambda_e, \lambda_0, P_e) = (-0.8, +1, -0.8)$ polarization configuration. In Figs.6-8 we plot the total cross section as a function of anomalous parameters for various final state polarizations. In these figures TR and LO stand for "transverse" and "longitudinal," respectively. We see from these figures that cross section is very small in the longitudinal polarization configuration. On the other hand, longitudinal polarization remarkably improves the deviations from the SM at the positive values of the parameter b_W . For instance, in Fig.7 longitudinal cross section increases by a factor of 12 as b_W increases from 0 to 0.21. But this increment is only a factor of 1.4 for the unpolarized case. The reason for this comes from the fact that the longitudinal cross section has a symmetric behavior in the positive and negative intervals of the parameter but the unpolarized graph shifts a little to the right. Longitudinal polarization also improves the deviations from the SM at both positive and negative values of β_W .

Angular distributions of the Higgs boson for unpolarized and longitudinally polarized cross sections are given in Figs.9 and 10. In the figures θ_H is the angle between the outgoing Higgs boson and the incoming electron in the center of mass frame of e^+e^- . Angular distributions for other polarization configurations are very similar to the unpolarized cross section. So we will not give them in the paper. One can see from Fig.10 that deviation of the differential cross section from its SM value is larger in the negative interval of $\cos \theta_H$.

III. LIMITS ON THE ANOMALOUS COUPLING PARAMETERS

For a concrete result we have obtained 95% C.L. limits on the anomalous coupling parameters a_W , b_W , and β_W using χ^2 analysis at $\sqrt{s} = 0.5$ and 1 TeV and integrated luminosity $L_{int} = 500 \text{ fb}^{-1}$ without systematic errors. In our calculations we choose to work with a

Higgs boson of mass 120 GeV. Therefore the dominant decay mode should be $H \rightarrow b\bar{b}$ with a branching ratio $B_H \approx 0.9$.

We assume that W polarization can be measured. Indeed angular distribution of the W decay products has a clear correlation with the helicity states of the W boson. Therefore we consider the case in which W momentum is reconstructible. We restrict ourselves to a $W \rightarrow q\bar{q}'$ decay channel with a branching ratio $B_W \approx 0.68$. The number of events are given by $N = EB_W B_H L_{int} \sigma$, where E is the b -tagging efficiency and it is taken to be 0.7 as Refs. [5, 8]. There have been several experimental studies in the literature for the measurement of W polarization. W boson polarization has been studied at the CERN e^+e^- collider LEP2 via the process $e^+e^- \rightarrow W^+W^- \rightarrow \ell\nu q\bar{q}'$ [15]. At Fermilab Tevatron, polarization of the W bosons produced in the top quark decay has been measured by the CDF and DØ collaborations [16].

Limits on the anomalous WWH couplings are given in Tables I and II for various initial and final polarization configurations. In the tables, $(\lambda_0, \lambda_e, P_e) = (0, 0, 0)$ is for unpolarized initial beams and TR+LO represents the unpolarized W boson. We take into account $(\lambda_0, \lambda_e, P_e) = (+1, -0.8, -0.8)$ initial polarization configuration which gives the largest deviation from the SM (Figs. 3-5). It can be seen from Fig.10 that deviation of the differential cross section from its SM value is larger in the negative interval of $\cos\theta_H$. So we impose a restriction $\cos\theta_H < 0$ on the longitudinal polarization configuration to improve the limits. We represent these restricted limits with a superscript " * ". We see from Table I that polarization leads to a significant improvement on the upper bound of b_W . Polarization improves the upper bound of b_W by a factor of 7.4. This improvement factor becomes 9.3 when we consider $\cos\theta_H < 0$ restriction. At $\sqrt{s} = 0.5$ TeV these improvement factors are smaller; we see from Table II that initial state polarization together with final polarization and $\cos\theta_H < 0$ restriction improve the upper bound of b_W approximately by a factor of 4.3. Polarization improves both upper and lower bounds of β_W . Improvement factors for upper and lower bounds are the same and equal to 2.2 at $\sqrt{s} = 1$ TeV and 1.9 at $\sqrt{s} = 0.5$ TeV. Final state polarizations do not improve the lower bound of b_W . But initial polarizations improve the lower bound of b_W by a factor of 1.7 at $\sqrt{s} = 1$ TeV and 1.6 at $\sqrt{s} = 0.5$ TeV.

Anomalous couplings were studied in [8] through the same process $e^-\gamma \rightarrow \nu_e W^- H$ at the linear order of anomalous couplings and $\sqrt{s} = 0.5$ TeV energy. Authors took into account initial electron and photon polarizations (λ_e and λ_0) before Compton backscattering but

they neglected initial electron beam polarization (P_e) and also the final state polarization. Imposing same acceptance cuts, we have confirmed the results of [8] for all combinations of the initial polarizations λ_e and λ_0 . The unpolarized cross section at the linear order and $\sqrt{s} = 0.5$ TeV energy is given by

$$\sigma = [2.86(1 + 2\Delta a_W) - 11.07 b_W] fb \quad (9)$$

where $\Delta a_W = a_W - 1$ and coefficient of the parameter β_W is zero at the linear order due to \hat{T} invariance of the total cross section. \hat{T} is the pseudo-time reversal transformation, one which reverses particle momenta and spins but does not interchange initial and final states. The term proportional to β_W is \hat{T} odd in the total cross section at the linear order. Therefore only the quadratic order terms for β_W contribute to the cross section. In [8] authors imposed some cuts and restrict themselves to an appropriate part of the phase space in order to see the effects of β_W . It is, however, irrelevant for our treatment since we have considered all anomalous terms in our calculations. Using cross section (9) authors set 3σ bounds on the anomalous coupling parameters Δa_W and b_W with an integrated luminosity of $500 fb^{-1}$. If we convert these bounds into 95% confidence level they are approximately $|\Delta a_W| < 0.026$ and $|b_W| < 0.013$. We see from Table II that the limit on Δa_W is very close to the limit at the linear order and quadratic order anomalous contribution leads to a slight improvement. On the other hand, different from the limits at the linear order, limits on b_W are not symmetric. The lower bound of b_W is improved slightly but the upper bound get worse markedly. This is very compatible with Figs. 4 and 7 where we observe that minima of the unpolarized graphs shift a little to the right.

In conclusion, polarization leads to a considerable improvement on the upper bound of the anomalous parameter b_W . It improves both upper and lower bounds of β_W . Although the SM cross sections in the longitudinal polarization configuration of the final W are small, sensitivity limits are better than the transverse polarization case. As mentioned in [5, 7] the process $e^- e^+ \rightarrow \nu \bar{\nu} H$ can be a good probe to measure the WWH coupling at high energies. The disadvantage of $e^- e^+ \rightarrow \nu \bar{\nu} H$ is that it also receive contributions from the ZZH vertex and with the final neutrinos being invisible this process has too few observables associated

with it. This makes it very difficult to dissociate WWH from ZZH [5].

- [1] R. Barate *et al.*, Phys. Lett. **B 565**, 61 (2003).
- [2] LEP Electroweak Working Group, <http://lepewwg.web.cern.ch/LEPEWWG/>.
- [3] C. Akerlof, Ann Arbor Report No. UM HE 81-59 (1981);
T.L. Barklow, in Proceedings of the 1990 Summer Study on Research Directions for the Decade (Snowmass, Colorado, 1990), and SLAC Report No. SLAC-PUB-5364 (1990);
J. A. Aguilar-Saavedra *et al.*, TESLA Technical Design Report Part III, DESY-2001-011.
- [4] I.F. Ginzburg *et al.*, Nucl. Instrum. Methods **205**, 47 (1983); *ibid.* **219**, 5 (1984).
- [5] S.S. Biswal, D. Choudhury, R.M. Godbole and R.K. Singh, Phys. Rev. **D73**, 035001 (2006).
- [6] M.C. Gonzalez-Garcia, Int. J. Mod. Phys. **A14**, 3121 (1999).
- [7] V. Barger, T. Han, P. Langacker, B. McElrath and P. Zerwas, Phys. Rev. **D67**, 115001 (2003).
- [8] D. Choudhury and Mamta, Phys. Rev. **D74**, 115019 (2006).
- [9] H.-J. He, Y.-P. Kuang, C.-P. Yuan and B. Zhang, Phys. Lett. **B 554**, 64 (2003);
B. Zhang, Y.-P. Kuang, H.-J. He and C.-P. Yuan, Phys. Rev. **D 67**, 114024 (2003).
- [10] V. Hankele, G. Klämke, D. Zeppenfeld and T. Figy, Phys. Rev. **D 74**, 095001 (2006).
- [11] M.C. Gonzalez-Garcia, S. M. Lietti and S. F. Novaes, Phys. Rev. **D59**, 075008 (1999).
- [12] T. Han, Y-P. Kuang and B. Zhang, Phys. Rev. **D 73**, 055010 (2006).
- [13] A. Ballestrero and E. Maina, Phys. Lett. **B350**, 225(1995).
- [14] T. Kaneko in *New Computing Techniques in Physics Research*, edited by D. Perret-Gallix, W. Wojcik (Edition du CNRS, Paris, 1990); MINAMI-TATEYA Group, KEK Report No. 92-19, 1993; F. Yuasa *et al.*, Prog. Theor. Phys. Suppl. **138** 18 (2000).
- [15] P. Achard *et al.* (L3 Collaboration), Phys. Lett. B **557**, 147 (2003); G. Abbiendi *et al.* (OPAL Collaboration), Phys. Lett. B **585**, 223 (2004); J. Abdallah *et al.* (DELPHI Collaboration), Eur. Phys. J. C **54**, 345 (2008).
- [16] V.M. Abazov *et al.* (DØ Collaboration), Phys. Lett. B **617**, 1 (2005); A. Abulencia *et al.* (CDF Collaboration), Phys. Rev. D **73**, 111103 (2006) ;Phys. Rev. D **75**, 052001 (2007).

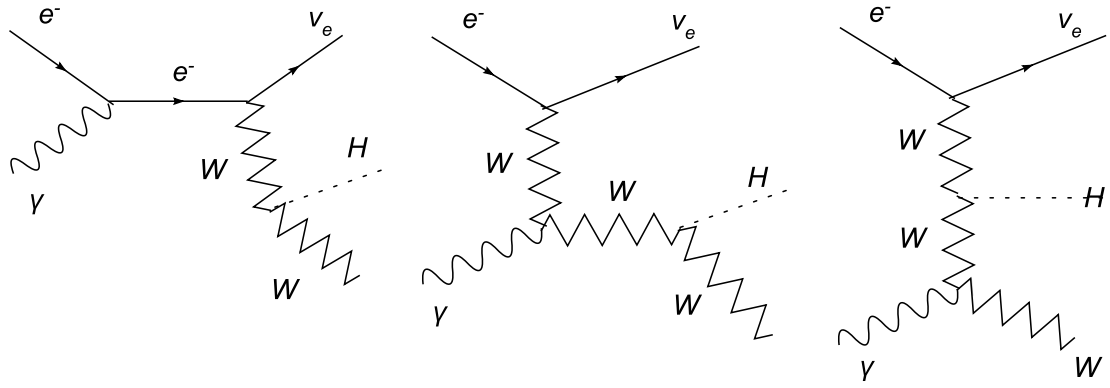


FIG. 1: Tree-level Feynman diagrams for $e^- \gamma \rightarrow \nu_e W^- H$.

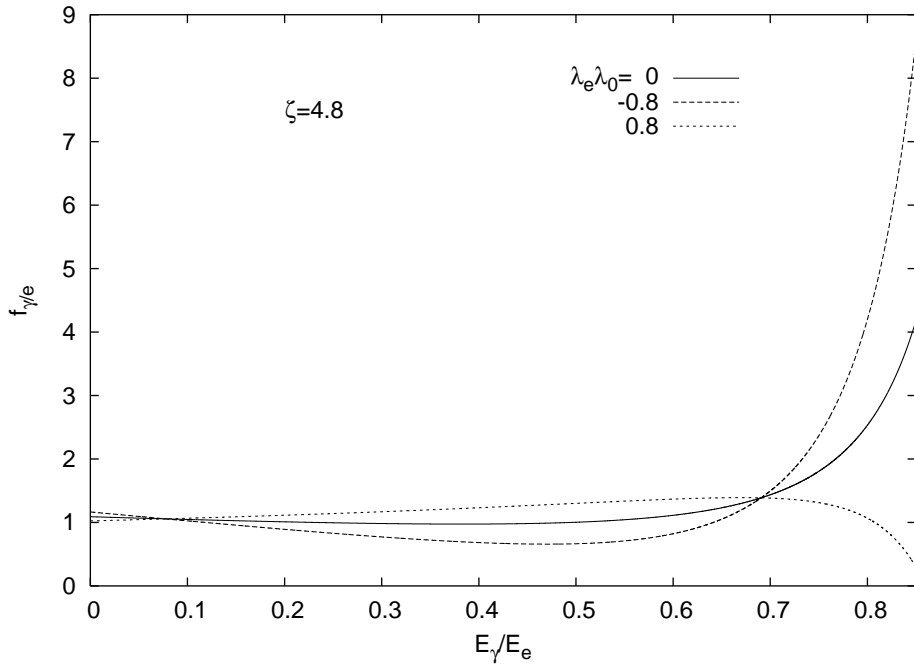


FIG. 2: Energy distribution of backscattered photons for $\lambda_e \lambda_0 = 0, -0.8, 0.8$.

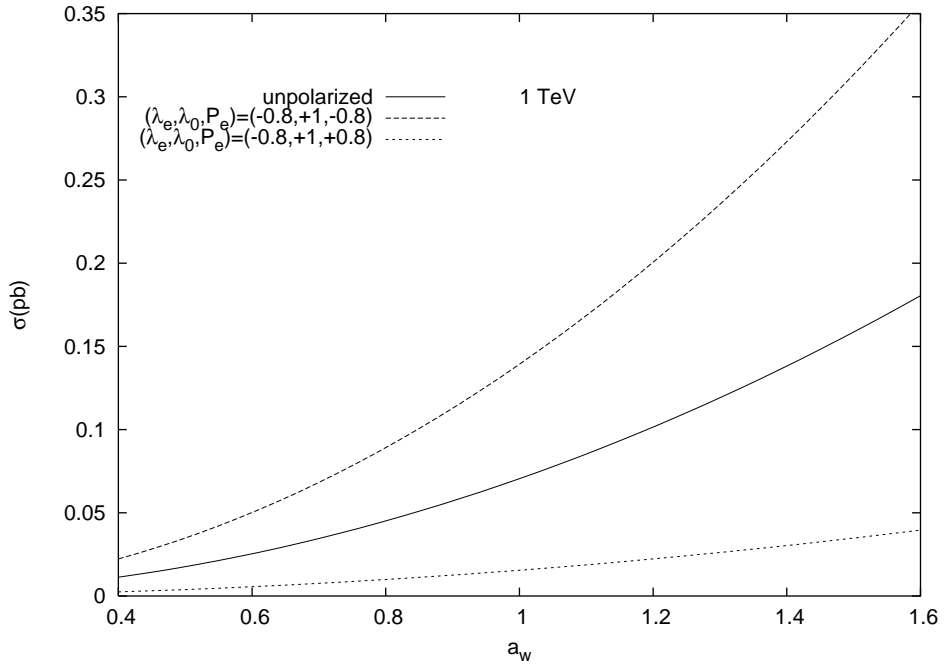


FIG. 3: The integrated total cross section of $e^- \gamma \rightarrow \nu_e W^- H$ as a function of anomalous coupling a_W . The legends are for initial beam polarizations. $\sqrt{s} = 1\text{TeV}$.

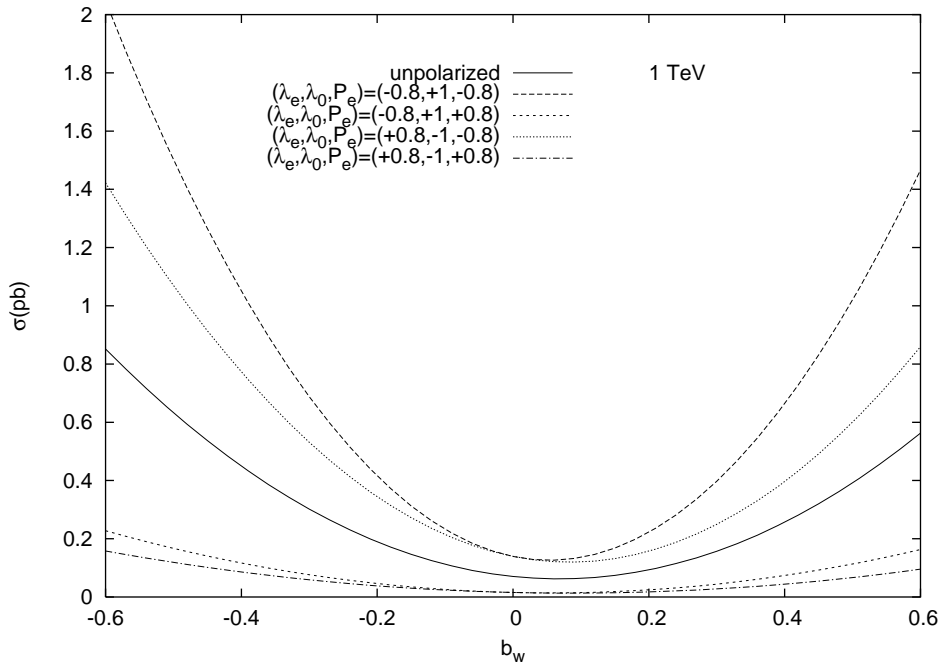


FIG. 4: The integrated total cross section of $e^- \gamma \rightarrow \nu_e W^- H$ as a function of anomalous coupling b_W . The legends are for initial beam polarizations. $\sqrt{s} = 1\text{TeV}$.

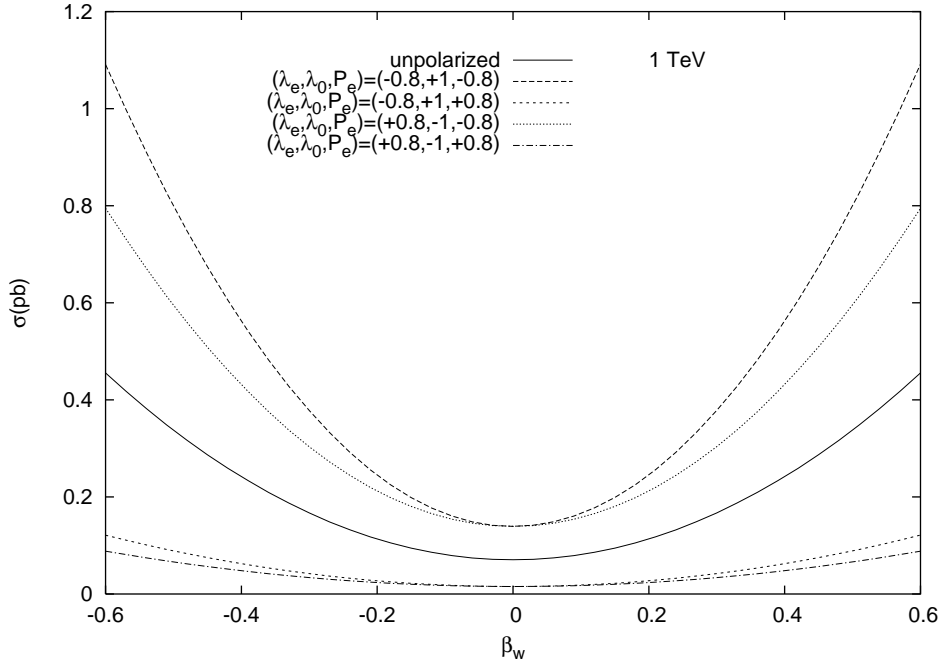


FIG. 5: The integrated total cross section of $e^-\gamma \rightarrow \nu_e W^- H$ as a function of anomalous coupling β_W . The legends are for initial beam polarizations. $\sqrt{s} = 1 TeV$.

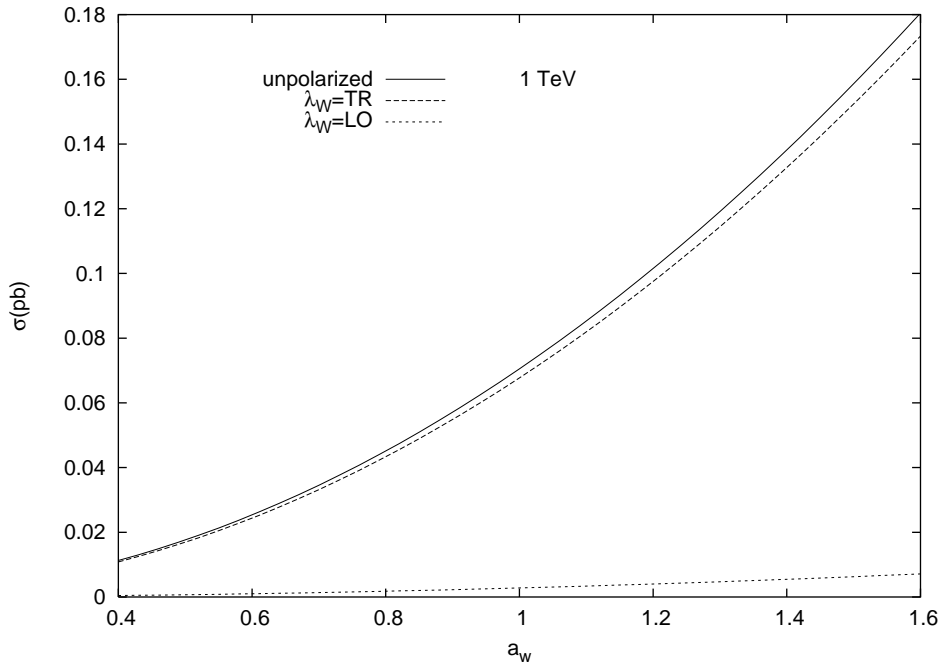


FIG. 6: The integrated total cross section of $e^-\gamma \rightarrow \nu_e W^- H$ as a function of anomalous coupling a_W . The legends are for final state polarizations. $\sqrt{s} = 1 TeV$.

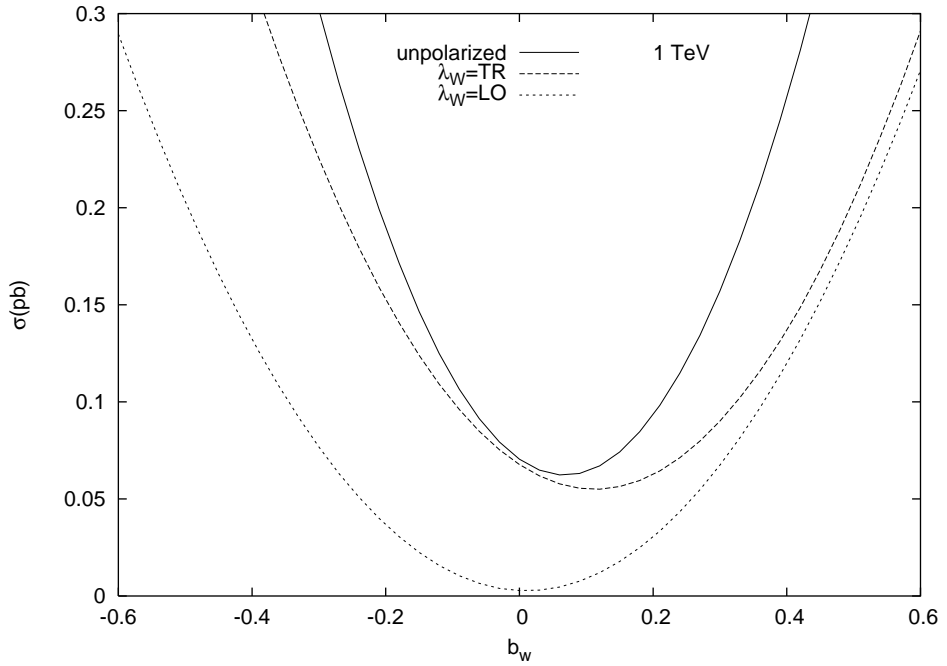


FIG. 7: The integrated total cross section of $e^- \gamma \rightarrow \nu_e W^- H$ as a function of anomalous coupling b_W . The legends are for final state polarizations. $\sqrt{s} = 1 \text{TeV}$.

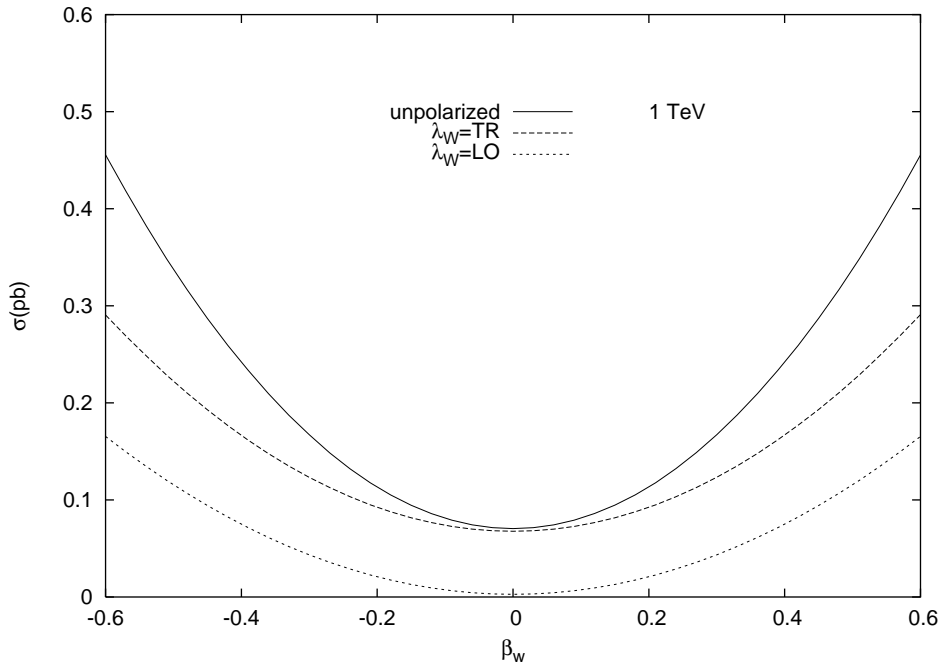


FIG. 8: The integrated total cross section of $e^- \gamma \rightarrow \nu_e W^- H$ as a function of anomalous coupling β_W . The legends are for final state polarizations. $\sqrt{s} = 1 \text{TeV}$.

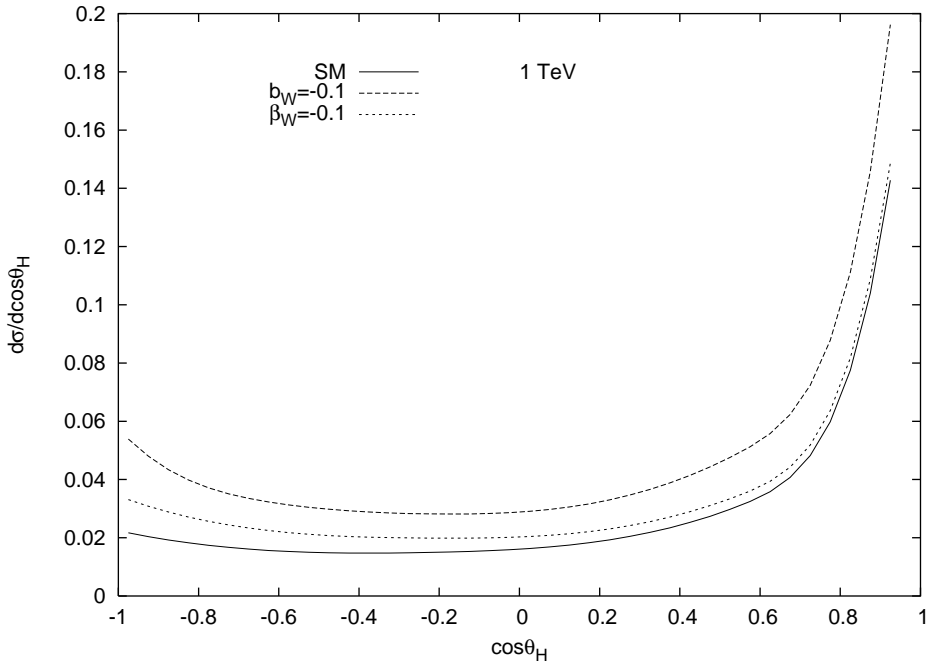


FIG. 9: Angular distributions of the Higgs boson in the center of the mass frame of e^+e^- for unpolarized beams. θ_H is the angle between the outgoing Higgs boson and the incoming electron.

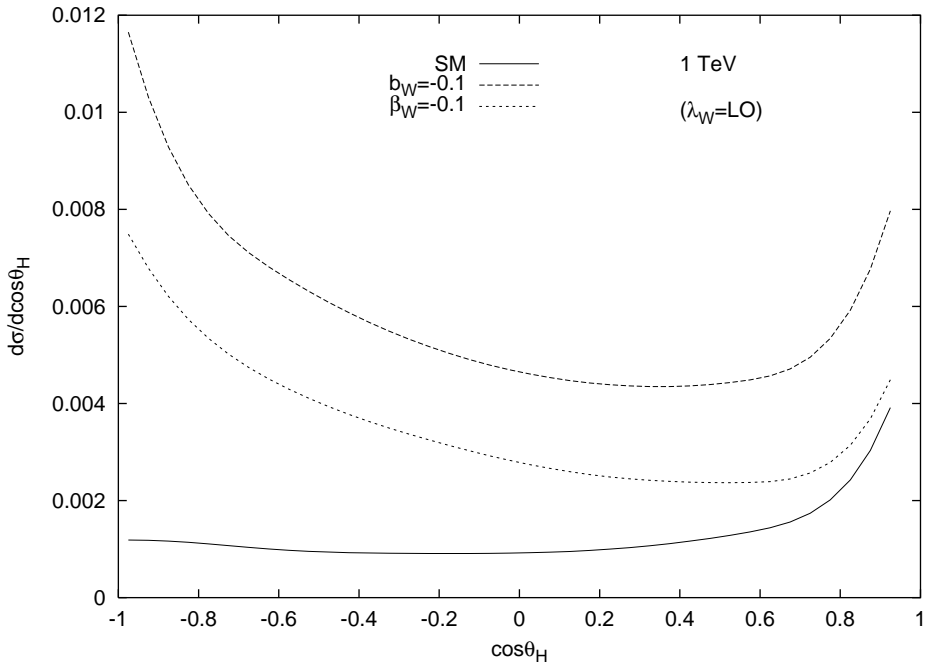


FIG. 10: Angular distributions of the Higgs boson in the center of mass frame of e^+e^- for the longitudinal polarization state of the final W .

TABLE I: Sensitivity of the $e\gamma$ collision to anomalous WWH couplings at 95% C.L. for $\sqrt{s} = 1$ TeV and $L_{int} = 500 \text{ fb}^{-1}$. The effects of final state W boson polarization and initial beam polarizations are shown in each row. The superscript " * " represents the restriction $\cos \theta_H < 0$ in the phase space.

λ_0	λ_e	P_e	λ_W	a_W	b_W	β_W
0	0	0	$TR + LO$	(0.992, 1.008)	(-0.005, 0.140)	(-0.033, 0.033)
0	0	0	TR	(0.992, 1.008)	(-0.005, 0.230)	(-0.043, 0.043)
0	0	0	LO	(0.960, 1.040)	(-0.010, 0.030)	(-0.023, 0.023)
0	0	0	LO^*	(0.931, 1.065)*	(-0.011, 0.022)*	(-0.020, 0.020)*
+1	-0.8	-0.8	$TR + LO$	(0.995, 1.006)	(-0.003, 0.111)	(-0.024, 0.024)
+1	-0.8	-0.8	TR	(0.995, 1.006)	(-0.003, 0.205)	(-0.033, 0.033)
+1	-0.8	-0.8	LO	(0.970, 1.030)	(-0.007, 0.019)	(-0.015, 0.015)
+1	-0.8	-0.8	LO^*	(0.953, 1.047)*	(-0.008, 0.015)*	(-0.014, 0.014)*

TABLE II: The same as Table I but for $\sqrt{s} = 0.5$ TeV.

λ_0	λ_e	P_e	λ_W	a_W	b_W	β_W
0	0	0	$TR + LO$	(0.980, 1.020)	(-0.011, 0.261)	(-0.078, 0.078)
0	0	0	TR	(0.980, 1.020)	(-0.012, 0.363)	(-0.098, 0.098)
0	0	0	LO	(0.930, 1.067)	(-0.018, 0.114)	(-0.067, 0.067)
0	0	0	LO^*	(0.865, 1.120)*	(-0.020, 0.087)*	(-0.060, 0.060)*
+1	-0.8	-0.8	$TR + LO$	(0.987, 1.014)	(-0.007, 0.206)	(-0.056, 0.056)
+1	-0.8	-0.8	TR	(0.986, 1.013)	(-0.008, 0.307)	(-0.085, 0.085)
+1	-0.8	-0.8	LO	(0.950, 1.050)	(-0.011, 0.077)	(-0.042, 0.042)
+1	-0.8	-0.8	LO^*	(0.910, 1.070)*	(-0.012, 0.061)*	(-0.058, 0.058)*